Spectral Modeling and Relighting of Reflective-Fluorescent Scenes

Antony Lam and Imari Sato

National Institute of Informatics

2-1-2 Hitotsubashi, Chiyoda, Tokyo 101-8430, Japan

`antony@nii.ac.jp, imarik@nii.ac.jp`

Abstract

Hyperspectral reflectance data allows for highly accurate spectral relighting under arbitrary illumination, which is invaluable to applications ranging from archiving cultural e-heritage to consumer product design. Past methods for capturing the spectral reflectance of scenes has proven successful in relighting but they all share a common assumption. All the methods do not consider the effects of fluorescence despite fluorescence being found in many everyday objects. In this paper, we describe the very different ways that reflectance and fluorescence interact with illuminants and show the need to explicitly consider fluorescence in the relighting problem. We then propose a robust method based on well established theories of reflectance and fluorescence for imaging each of these components. Finally, we show that we can relight real scenes of reflective-fluorescent surfaces with much higher accuracy in comparison to only considering the reflective component.

1. Introduction

Hyperspectral reflectance data has been used for highly accurate spectral relighting of scenes under arbitrary illumination and has benefited many applications ranging from archiving for cultural e-heritage to the design of consumer products. In fact, previous research has demonstrated the necessity of using spectral reflectance for accurate relighting [7, 16, 24]. Thus there have been many methods for imaging the spectral reflectance of scenes [3, 4, 10, 14, 21].

While previous methods for measuring spectral reflectance have been successful in accurately predicting the color of objects under arbitrary illumination, they all make the same assumption that fluorescence is absent from the scene. This is despite the fact that fluorescence is a common phenomenon observed in many objects. In fact, Barnard showed through intensive studies on color constancy algorithms, that fluorescent surfaces are common and present in 20% of randomly constructed scenes [2]. In addition, Johnson and Fairchild also showed how the appearance of a
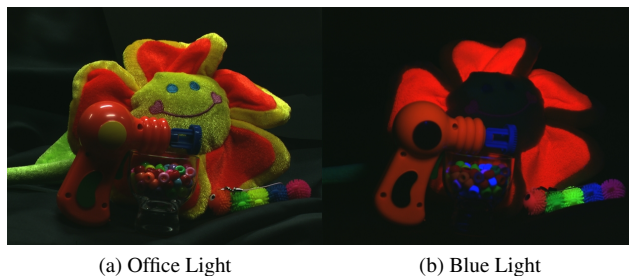

(a) Office Light   (b) Blue Light

Figure 1: Scene under two illuminantions. Fluorescence has a wavelength shifting property that can cause orange to appear under blue light.

composite object with both fluorescent and reflective components dramatically changes under different illumination in computer graphics [7].

More importantly, reflective and fluorescent components interact with illuminants differently. Reflective surfaces emit light at the same wavelength as the light source but fluorescent surfaces will first absorb incident light and then emit at longer wavelengths–a phenomenon known as Stokes shift [17, 19]. Fig. 1 illustrates this wavelength shifting phenomenon where under blue light, orange can be observed.

In this paper, we present a new relighting method where we focus on the issues of accurately modeling and predicting the color of a scene in the presence of fluorescence. We start by detailing exactly how reflectance and fluorescence are different. We then present our method for capturing various spectral domain characteristics of reflective-fluorescent scenes for accurate relighting. Specifically, we devise an imaging process that first extracts the reflectance only component of a scene. Then using the reflectance data, we extract two components of fluorescence called the emission and excitation which are crucial for accurate modeling and relighting of fluorescent surfaces. Essentially, the excitation models how incoming light is absorbed and the emission models how light is emitted. Relighting under arbitrary illumination can then be done based on the recovered reflective and fluorescent components.

We also note that to our knowledge, we are the first to introduce a method for modeling and relighting of scenes with both reflective and fluorescent components based on well established theories and observations of the physical behaviors of said components. Our consideration of fluorescence provides much better predictions of how colors appear when relighted in comparison to only considering the reflective component.

The main contributions of this paper are that we

1. Introduce the very different behaviors between reflectance and fluorescence and show the need for explicit joint modeling of the two phenomenon.

2. Propose a robust method for estimating the three spectral components of reflective-fluorescent scenes using sparsely captured band images.

3. Show that fluorescent components can be modeled using sets of spectral basis vectors that well represent the excitation and emission of fluorescent materials.

4. Demonstrate that our models allow for correct synthesis of real scene appearances under novel lighting.

1.1. Related Work

Past methods have been effective for estimating the spectral reflectance of scenes. For example, Maloney and Wandell used a three-channel camera for spectral reflectance recovery under ambient light [10]. Tominaga later introduced the use of a multi-channel camera for spectral reflectance illuminant recovery by sequentially placing band-pass filters in front of a monochromatic camera [21]. Another popular alternative is the use of tunable filters to obtain multispectral images [5].

Other researchers proposed the use of active illumination for spectral reflectance recovery. Park *et al.* used multiplexed illumination emitted by sets of LEDs for fast spectral imaging of dynamic scenes [14]. In Chi *et al.* [3], optimized wide band filtered illumination allowed a conventional camera to obtain spectral information of a scene in the presence of unknown ambient illumination. Ultimately, these methods have their own strengths but none consider the effects of fluorescence.

Considering fluorescence does add a layer of complexity. One notable paper aimed to overcome the complexity by approximating fluorescent effects through a data driven simplified model for relighting [2]. However, their model does not properly account for exactly how reflectance and fluorescence would interact with incoming light. On the other hand, research in fluorometry details proper procedures for measuring the color of fluorescent materials in the spectral domain using optical devices [20]. For example, bispectral methods are well established approaches to measuring the spectral distribution of the fluorescence as a function of incident and outgoing wavelengths for a single point. Unfortunately, measuring all points in a scene is a difficult task

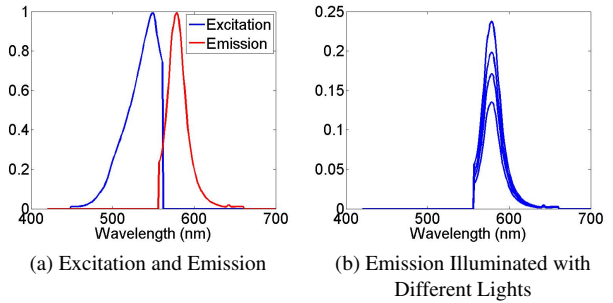(a) Excitation and Emission   (b) Emission Illuminated with Different Lights

Figure 2: Sample Excitation and Emission Spectra

that would require densely sampling in both the spectral and spatial domains. We will overcome this difficulty by the use of real-world statistics that allow for full recovery of all spectra in a scene using sparsely captured band images.

It is notable that Hullin *et al.* acquire bispectral bidirectional reflectance and reradiation distribution functions (BRRDF) of fluorescent objects using a sampling strategy on spheres with fluorescent paint [6]. They demonstrated the effectiveness of modeling and rendering fluorescent objects but their method requires precise bispectral and bidirectional measurements of object appearance, and is thus not suitable for modeling and relighting an entire scene.

Regarding the separation of reflective and fluorescent components, Alterman *et al.* proposed separating the appearance of each fluorescent dye from a mixture by unmixing multiplexed images [1]. In Zhang and Sato [26], a detailed model for reflectance and fluorescence was presented and used to accurately separate reflective and fluorescent components from scenes. These methods successfully separate fluorescent components, but do not fully model the reflective and fluorescent components of a scene and so cannot be used for spectral relighting. Recently, Tominaga *et al.* proposed a method for estimating the emission spectra of fluorescence using multi-spectral images taken under two ordinary light sources. However, they assume that fluorescent emission is constant for all excitation wavelengths and thus cannot accurately predict the brightness of fluorescent components under varying illumination [22].

2. Reflectance and Fluorescence

As discussed, illuminated reflective surfaces emit light at the same wavelength as the light source while fluorescent surfaces absorb incident light and then emit at longer wavelengths. Despite the very different natures of reflectance and fluorescence, many materials contain both components. Thus accurate relighting of such surfaces requires a model that jointly considers both effects. We begin by considering such a model in its most general form. The appearance of a reflective-fluorescent surface point at wavelength λ_o illuminated at wavelength λ_i can be expressed as a linear

combination of the reflective and fluorescent components.

$$P(\lambda_o, \lambda_i) = P_R(\lambda_o, \lambda_i) + P_F(\lambda_o, \lambda_i) \qquad (1)$$

where $P_R(\lambda_o, \lambda_i)$ and $P_F(\lambda_o, \lambda_i)$ are the reflective and fluorescent terms computed from information on the surface point's physical properties and illuminant I at wavelength λ_i.

As mentioned, reflectance emits light at the same wavelength as the illuminant so it's model is expressed as

$$P_R(\lambda_o, \lambda_i) = R(\lambda_o)I(\lambda_i)\delta(\lambda_o - \lambda_i) \qquad (2)$$

where $R(\lambda_o)$ is the reflectance at wavelength λ_o and $I(\lambda_i)$ is the illuminant at wavelength λ_i. $\delta(\cdot)$ is the unit impulse function where $\delta(0) = 1$ and $\delta(x) = 0$ for $x \neq 0$.

The fluorescent term is more complex and is expressed in terms of different functions for how incoming light "excites" the material and what light is "emitted."

$$P_F(\lambda_o, \lambda_i) = Em(\lambda_o)Ex(\lambda_i)I(\lambda_i) \qquad (3)$$

where $Em(\lambda_o)$, $Ex(\lambda_i)$, and $I(\lambda_i)$ are the emission, excitation, and illuminant at their respective wavelengths. Fig. 2a shows examples of excitation and emission spectra for one fluorescent dye over the visible spectrum. Also, the emission being to the right of the excitation is an example of Stokes shift.

Up to this point, we have only described reflectance and fluorescence under narrowband illumination. In the case of wideband illumination, the emitted light at wavelength λ_o is expressed as a sum over all illumination wavelengths λ_i.

$$\begin{aligned} P(\lambda_o) &= \int P(\lambda_o, \lambda_i)d\lambda_i \\ &= R(\lambda_o)I(\lambda_o) + Em(\lambda_o)\int Ex(\lambda_i)I(\lambda_i)d\lambda_i \end{aligned} \qquad (4)$$

We now bring attention to an interesting and well known phenomenon that was detailed in Zhang and Sato [26]. It can be seen from Eq. 4 that for a fixed illumination, $\int Ex(\lambda_i)I(\lambda_i)d\lambda_i$ is a constant that is independent of the outgoing wavelength λ_o being observed. Thus in the absence of the reflective component $R(\lambda_o)I(\lambda_o)$, the fluorescent emission spectrum would only be scaled by the amount of energy from the light source and how it interacts with the excitation. From this, the observed spectrum would have the same distribution of values over all wavelengths regardless of the illuminant. See Fig. 2b for an example.

3. Overview of Reflectance and Fluorescence Capture Process

In order to properly analyze the different components of reflectance, emission, and excitation described earlier, we need to be able to separate them. We accomplish this by imaging the three components using various combinations

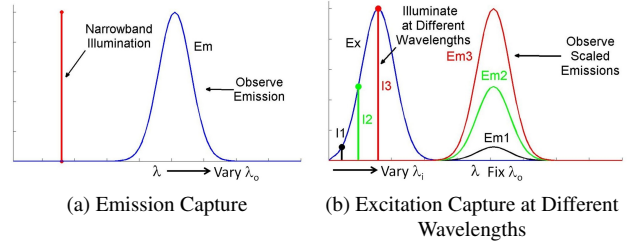(a) Emission Capture   (b) Excitation Capture at Different Wavelengths

Figure 3: Capture of fluorescent components for a single point. We extend these basic ideas to simultaneously capture the same components for all points in a scene and use them to render relighting in RGB.

of illuminants and filters. To put our method into the proper context, we first briefly discuss how imaging the three components could be done for a single point.

Reflectance Capture: Due to Stokes shift, a fluorescent point illuminated at wavelength λ_i will generally emit light at longer wavelengths λ_o. This means that if we illuminate a reflective-fluorescent point at λ_i and observe the point at λ_o when $\lambda_i = \lambda_o$, we will observe only the reflective component.

Emission Capture: The illuminant only changes the scaling of the emission spectrum and so the shape of the emission is invariant to incident light. Thus if we fix an illuminant at λ_i, the emission could be observed for any wavelength $\lambda_o > \lambda_i$.[1] We would only need to vary λ_o to observe the entire emission spectrum. For a reflective-fluorescent point, no reflectance would be observed at λ_o since reflectance only emits at the same wavelength as the illuminant. Fig. 3a shows an emission illuminated by a narrowband light.

Excitation Capture: We can observe the emission at a wavelength λ_o while we varying the illuminant wavelength λ_i for $\lambda_i < \lambda_o$. This would allow us to observe how much different wavelengths of light would rescale the emission which by definition is the excitation spectrum. Fig. 3b shows the observation of different scaled emissions to infer excitation at the illuminant wavelength.

In general, a scene consists of multiple fluorescent materials so it is difficult to fix λ_i or λ_o to observe all fluorescent spectra. We propose a solution to this issue in Secs. 4.2 and 4.3 by using wideband light and a wideband camera to observe the scene.

4. Imaging the Reflective Component

As mentioned, due to Stokes shift, when the point is both illuminated and observed at the same wavelength, we will see only the reflective component. Thus if we use a nar-

---

[1]This fact has been used for shape recovery based on fluorescent components [18, 23].

rowband light source at wavelength λ and capture the scene using a camera equipped with a narrowband filter that only allows wavelength λ through, we can capture the reflectance of the scene at λ. Specifically, the model of such a process can be expressed as $M_p = R(\lambda)I(\lambda)c(\lambda)f(\lambda)$ where $c(\lambda)$ and $f(\lambda)$ are the camera and filter sensitivities at wavelength λ. If we then divide out $I(\lambda)c(\lambda)f(\lambda)$, we would have reflectance $R(\lambda)$. Provided this process is repeated for all wavelengths, the full reflectance spectra could be obtained. However, this would be labor intensive and time consuming since high exposure times are typically needed to reduce noise. In the next subsection, we derive a method that can make use of real-world statistics on spectra to accurately estimate a full spectrum given only a few sparse values of the spectrum at different wavelengths.

4.1. Recovering Full Reflectance Spectra using Sparse Wavelengths

It is well known reflectance spectra from various domains such as Munsell colors and natural scenes can be treated as vectors and represented compactly using 6-8 principal components derived from real world statistics [8, 9, 11, 15]. Therefore spectral reflectance $R(\lambda)$ can be represented as a linear combination of orthonormal basis vectors as $R(\lambda) = \sum_{i=1}^{N} \sigma_n b_n(\lambda)$ where $b_n(\lambda)$ is the nth basis vector at wavelength λ, and σ_n is the coefficient associated with basis b_n.

If we consider the wavelengths λ to be discrete and restricted to a fixed range, we can express the basis representation of $R(\lambda)$ in matrix form as $\vec{r} = \mathbf{B}\vec{\sigma}$ where $\vec{r}$ is a vector of the $R(\lambda)$ values for all λ, $\mathbf{B}$ is the orthonormal column matrix of basis vectors, and $\vec{\sigma}$ is the vector of coefficients.

We now describe how a sparse set of wavelength measurements of spectrum R fits into our framework which was inspired by [12] and [6] where they solved different problems but used a similar analysis. Let $\vec{r'}$ be sparse measurements whose entries are the same as $\vec{r}$ for the observed wavelengths and zeros elsewhere. If we project $\vec{r}$ onto basis $\mathbf{B}$, we get coefficients $\vec{\sigma} = \mathbf{B}^T\vec{r}$ while projecting $\vec{r'}$ onto basis $\mathbf{B}$ would give coefficients $\vec{\sigma'} = \mathbf{B}^T\vec{r'}$.

To see the connection between $\vec{\sigma}$ and $\vec{\sigma'}$, we now define a matrix $\mathbf{B'}$ as the sparse basis version of matrix $\mathbf{B}$. Specifically, the rows of $\mathbf{B'}$ that correspond to the selected wavelengths are the same as $\mathbf{B}$ while all other rows are zero. It can then be shown that $\vec{\sigma'} = \mathbf{B}^T\vec{r'} = (\mathbf{B'})^T\vec{r'} = (\mathbf{B'})^T\vec{r} = (\mathbf{B'})^T\mathbf{B}\vec{\sigma}$. Which implies that $\vec{\sigma} = ((\mathbf{B'})^T\mathbf{B})^+\vec{\sigma'}$ where "+" is the pseudoinverse. Thus given sparse wavelengths $\vec{r'}$ we can compute $\vec{r}$ as

$$\vec{r} = \mathbf{B}((\mathbf{B'}^T\mathbf{B})^+\mathbf{B}^T\vec{r'} \qquad (5)$$

The full spectrum $\vec{r}$ is accurately estimated through a selection of good sparse wavelengths to use.

The key to getting a good approximation of the full spectrum $\vec{r}$ from sparse measurements is to select sparse wavelengths so that the pseudoinverse in Eq. 5 would be stable. So if we select sparse wavelengths such that the condition number of $(\mathbf{B'})^T\mathbf{B}$ is close to 1, we will have a good approximation. An exhaustive search of the solution space would be time consuming so we adapted the greedy approach described in Matusik *et al.* [12]. The procedure operates as follows

1. Randomly select n wavelengths to be in set S. Place all other wavelengths in set O.
2. Create a matrix $\mathbf{B'}$ for the selected wavelengths S as described earlier.
3. Evaluate the condition number of $(\mathbf{B'})^T\mathbf{B}$.
4. Randomly select one wavelength $s \in$ S and one wavelength $o \in$ O and swap their set memberships.
5. Create matrix $\mathbf{B'}$ again and evaluate the condition number of $(\mathbf{B'})^T\mathbf{B}$.
6. If the newer condition number is greater than the previous condition number, swap s and o back to their original sets.
7. Repeat from step 4 until the condition number does not change.

While this procedure is greedy, we have found via comparison to exhaustive search that five random restarts of this greedy procedure always yields the optimal results for n = 1 to 8 in the case of reflectance spectra.

4.2. Fluorescent Emission Capture

Let us start from the simplest case where a scene consists of a homogeneous fluorescent material. As described in Sec. 3, its emission spectrum can be easily obtained by illumination at an appropriate narrowband wavelength λ_i and capture of its emitted light for all wavelengths $\lambda_o > \lambda_i$. The model for imaging based on this process can be expressed as $M_F = Em(\lambda_o)Ex(\lambda_i)I(\lambda_i)c(\lambda_o)f(\lambda_o)$ where $c(\lambda_o)$ and $f(\lambda_o)$ are the camera and filter responses at their respective wavelengths. If we then divide out $I(\lambda_i)$, $c(\lambda_o)$, and $f(\lambda_o)$, we obtain $Em(\lambda_o)Ex(\lambda_i)$. If this imaging procedure is repeated for all wavelengths by varying λ_o, we can obtain Em up to scale $Ex(\lambda_i)$.

Fortunately, the laborious capture of all wavelengths is unnecessary because similar to the reflectance case, we have found that emission spectra can also benefit from our sparse wavelength algorithm described in Sec. 4.1. We have found that a large collection of emission spectra from the McNamara and Boswell Fluorescence Spectra Dataset [13] can be well represented using 12 principal components. Specifically, the top 12 eigenvectors can capture 99% of the variance in the McNamara and Boswell Dataset's emission spectra. In addition, we tested the 12 eigenvectors ability

to reconstruct spectra obtained from a real fluorescent chart with 17 colors using the following error metric

$$\left(\int (a(\lambda) - b(\lambda))^2 d\lambda \right) \Big/ \int a(\lambda)^2 d\lambda \qquad (6)$$

where a and b are the ground truth and reconstructed spectra respectively.

The reconstruction errors can be seen in Table 1. It can be seen that both the McNamra and Boswell Dataset (used to derive the basis) and the fluorescent chart show low errors. Thus our observed emission spectrum can be well represented as a linear combination of basis vectors by setting $Ex(\lambda_i)Em(\lambda_o) = Ex(\lambda_i) \sum_{i=1}^{N} \sigma_n b_n(\lambda_o)$ where $b_n(\lambda_o)$ is the nth basis vector at wavelength λ_o and σ_n is the coefficient associated with basis b_n. Similar to the reflectance case, we could then find a small condition number for $(\mathbf{B}')^T\mathbf{B}$ using the algorithm in Sec. 4.1 to utilize our method for recovering full emission spectra using only sparsely captured wavelengths.

When imaging a real scene though, materials could contain both reflectance and fluorescence. Furthermore, not all fluorescent materials necessarily excite at the same wavelength. To overcome these difficulties, we first subtract out reflectance and then propose an alternative imaging approach for emission capture. We utilize wideband light instead so that all emission spectra in the scene can be simultaneously excited by the same illuminant. In addition, a wideband illuminant provides another advantage that it would make emissions stronger than those illuminated at narrowbands.

Let us consider Eq. 4 which describes the appearance of a surface point at wavelength λ_o illuminated by wideband light I. Since we know the R component, we can first subtract out the reflectance term to obtain pure fluorescence. As a result, it is possible to image $Em(\lambda_o) \int Ex(\lambda_i)I(\lambda_i)d\lambda_i = k_{ex}Em(\lambda_o)$ since the lighting and excitation are constant. Varying the value of λ_o would give us the emission spectrum. Note that although we obtain the emission up to a scaling factor k_{ex}, the constant k_{ex} will be canceled during relighting as described in Sec. 5.

Our sparse wavelength method can also be applied in this case. This is because similar to the homogeneous fluorescent scene, we can estimate $Em(\lambda_o)$ up to the scaling factor k_{ex} by representing $Em(\lambda_o)$ using a basis. So $k_{ex}Em(\lambda_o) = k_{ex} \sum_{i=1}^{N} \sigma_n b_n(\lambda_o)$.

4.3. Fluorescent Excitation Capture

Like in Sec. 4.2, let us first consider the simple case of a homogeneous fluorescent material. In Sec. 4.2, we showed that it was possible to compute $Em(\lambda_o)Ex(\lambda_i)$ from an imaging process. To observe Em, we varied λ_o while fixing the value of λ_i. To observe Ex, we would vary λ_i

	McNamara & Boswell	Fluorescent Chart
Emission	0.009	0.005
Excitation	0.009	0.006

Table 1: Average Reconstruction Errors using Emission and Excitation Spectrum Bases on Different Datasets

while fixing the value of λ_o instead. Also, similar to the emission case, we have found that 12 principal components can represent 99% of the energy in excitation spectra from the MacNamara and Boswell Fluorescence Spectra Dataset well. We also show in Table 1 that reconstruction errors on the both the McNamara and Boswell Dataset and the fluorescent color chart were low. So we can express the observed excitation as a linear combination of basis vectors $Ex(\lambda_i)Em(\lambda_o) = Em(\lambda_o) \sum_{i=1}^{N} \sigma_n b_n(\lambda_o)$ and use sparse wavelengths derived from a large excitation dataset to estimate Ex scaled by $Em(\lambda_o)$.

Unfortunately, a scene can still contain many different emission spectra that may not even overlap meaning that we cannot obtain all excitation spectra from the scene by observing only one wavelength λ_o.

Fortunately, there is a workaround that avoids this issue. If we image using a wideband monochrome camera with response c and subtract out reflectance, the appearance of the surface point under narrowband light at λ_i is $M_f = \int Em(\lambda_o)c(\lambda)d\lambda_o Ex(\lambda_i)I(\lambda_i) = k_{em}Ex(\lambda_i)I(\lambda_i)$ since $\int Em(\lambda_o)c(\lambda_o)d\lambda_o$ is a constant. λ_i could again be varied to observe the entire spectrum Ex scaled by k_{em}. Note that the scale factor k_{em} will be canceled out in Sec. 5. Also, similar to emission spectra we can express excitation as a linear combination of basis vectors. So that $k_{em}Ex(\lambda_i) = k_{em} \sum_{i=1}^{N} \sigma_n b_n(\lambda_i)$. Therefore, our sparse wavelength algorithm could be employed to capture the full excitation spectra from images captured at only a few wavelengths.

5. Using the Spectra to Relight for RGB

We now present the relighting procedure for RGB images. We start by considering how a spectrum of light appears as pixel values in the red channel of a RGB camera.

$$\begin{aligned} R_p &= \int P(\lambda_o)c_R(\lambda_o)d\lambda_o \\ &= \int R(\lambda_o)I(\lambda_o)c_R(\lambda_o)d\lambda_o \\ &+ \int Em(\lambda_o)c_R(\lambda_o)d\lambda_o \int Ex(\lambda_i)I(\lambda_i)d\lambda_i \end{aligned} \qquad (7)$$

where $c_R(\lambda_o)$ is the camera's response in the red channel at wavelength λ_o. We have the reflectance R, so that could simply be plugged into Eq. 7 to determine the reflectance component in the red channel.

Using the emission Em and excitation Ex terms is not immediately obvious. This is because we captured both Em

and Ex up to different scale factors. For the purposes of rendering RGB images we overcome this issue as follows:

1. Compute normalized spectra Em' and Ex' such that $\int Em'(\lambda_o)d\lambda_o = 1$ and $\int Ex'(\lambda_i)d\lambda_i = 1$.
2. Compute k so that the imaged emission from Sec. 4.2 $k_{ex}Em(\lambda_o) = k(Em'(\lambda_o)) \int Ex'(\lambda_i)I(\lambda_i)d\lambda_i$.

where I is the illuminant used to image $k_{ex}Em$.

To relight, we can compute the appearance of a surface point under any new lighting I' for the red channel by

$$
\begin{aligned}
R_p &= \int R(\lambda_o)I'(\lambda_o)c_R(\lambda_o)d\lambda_o \\
&+ k\int Em'(\lambda_o)c_R(\lambda_o)d\lambda_o \int Ex'(\lambda_i)I'(\lambda_i)d\lambda_i
\end{aligned}
\tag{8}
$$

Similar equations are used for relighting the green and blue channels.

6. Experiments

In our experiments, we capture all images using a Hamamatsu ORCA Flash 2.8 monochrome camera. For observing narrowband light, we used a CRi VariSpec filter which allows for selectively allowing any narrowband light in the visible spectrum through to the camera. In cases where we needed to image wideband light, we simply removed the filter from the camera. For our light sources, we used a Nikon Equalized Light Source to produce all narrowband and wideband illuminants.

In our results, we first show that our method for estimating a full spectrum using sparse measurements at key wavelengths is accurate by comparing against brute force capture of all wavelengths. We then show that our estimated R, Em, and Ex spectra from sparse wavelength imaging yields highly accurate color relighting of scenes.

6.1. Estimating Full Spectra using Sparse Wavelengths

To compute a reflectance basis, we looked to the CAVE Multispectral Database [25]. PCA was then used to determine six top basis vectors characteristic of spectra in the database.[2] The algorithm in Sec. 4.1 was then used to find six sparse wavelengths for accurate recovery of full reflectance spectra. Recall that ideally, $(\mathbf{B}')^T\mathbf{B}$ should have a condition number of 1. We were able to find a $(\mathbf{B}')^T\mathbf{B}$ matrix with a condition number of 1.5 by selecting sparse wavelengths at 440, 490, 530, 580, 620, and 680 nm. For emission, we found that wavelengths at 420, 440, 460, 480, 500, 520, 550, 570, 590, 620, 660, and 690 nm resulted in a condition number of 3.8. For excitation, wavelengths 420, 430, 440, 460, 470, 490, 510, 530, 560, 570, 610, and 660 nm yielded a condition number of 6.3.

---

[2] The choice of six top eigenvectors is in agreement with studies on spectra in the literature as mentioned in Sec. 4.1.

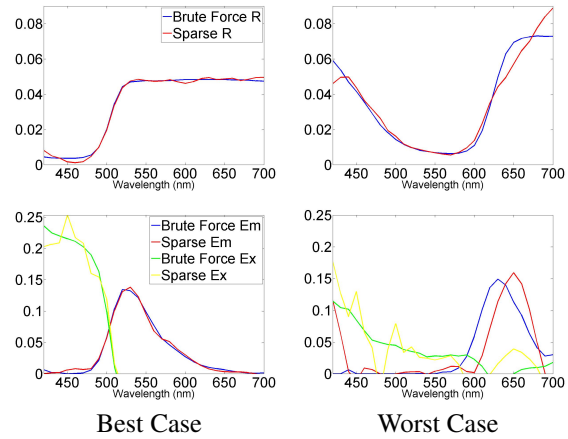| Reflectance	Emission	Excitation
0.004	0.045	0.064

Mean Errors

Best Case   Worst Case

Figure 4: Brute force versus sparse wavelength imaging of spectra on color charts. Despite the worst case having a poorly estimated Ex we found that the error had little effect on relighting performance. The mean errors between sparse wavelength and brute force imaging are shown at the top.

Since we image from 420 nm to 700 nm in increments of 10 nm, the brute force capture of all such wavelengths would require 29 images each for capturing R, Em, and Ex. In other words, a total of 87 images would be needed. Using our sparse wavelength approach reduces the required number of images to 30 for capturing all three components.

For our quantitative analysis, we used a standard MacBeth color checker and a color chart containing reflective-fluorescent paints. We then computed errors between brute force captured spectra from the charts and sparsely captured ones using Eq. 6 where a and b from the equation are the brute force and sparsely imaged spectra respectively.

Fig. 4 shows mean errors for the different spectra on the color charts. Reflectance spectra are very accurately estimated. Accurate reflectance estimation is crucial for our method because subsequent steps in capturing the fluorescent components depend on accurately subtracting out reflectance. Fig. 4 also shows best and worst case estimates from sparse wavelength measurements. The main source of error comes from estimating Ex and in the worst case, we encountered a peculiar Ex that was difficult to estimate. Fortunately, despite the error, Ex in this case was still accurate enough for relighting under a large number of wideband illuminants.

6.2. Relighting Scenes

We continue our quantitative analysis on the color chart scene by relighting it under three illuminants and show that the predicted colors are very close to ground truth images.

Reflective-Fluorescent Chart		Macbeth Chart	
	R+F	R Only	R+F	R Only
Blue Light	0.017	0.170	0.008	0.001
Green Light	0.012	0.069	0.005	0.007
D250 Light	0.003	0.056	0.002	0.003

Table 2: Mean Euclidean distances between predicted xy chromaticity and ground truth. The "R+F" means reflectance and fluorescence were considered. "R Only" means only reflectance was considered. The Macbeth chart is virtually pure reflectance so errors are small in both columns.

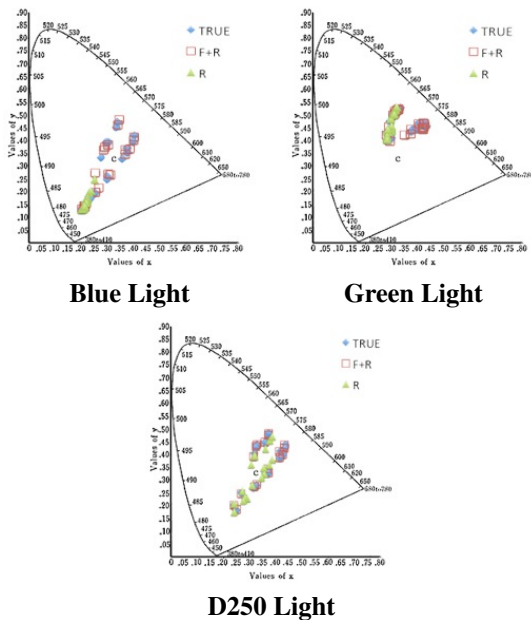
Blue Light   **Green Light**

D250 Light

Figure 5: Reflective-fluorescent chart xy chromaticities plotted. Blue diamonds are ground truth, red considers both reflectance and fluorescence, and green is relighting only with reflectance. Reflectance only relighting is incorrect in many cases.

Specifically, we rendered RGB images under blue, green, and the CIE D250 light. To measure our relighting's color accuracy, we computed xy chromaticity values from the rendered RGB values for each color on the chart and computed Euclidean distances to the ground truth. The same analysis was also done for the reflectance only component case. Table 2 shows the mean distances of our predicted colors from ground truth images. In the case of the Macbeth chart, since the colors are virtually pure reflectance, there is little difference between our method and considering only reflectance. For the reflective-fluorescent chart, we see that considering fluorescence reduces the error. The advantage is even more apparent in Fig. 5 which shows the chromatic-

Ground Truth Under Different Lighting
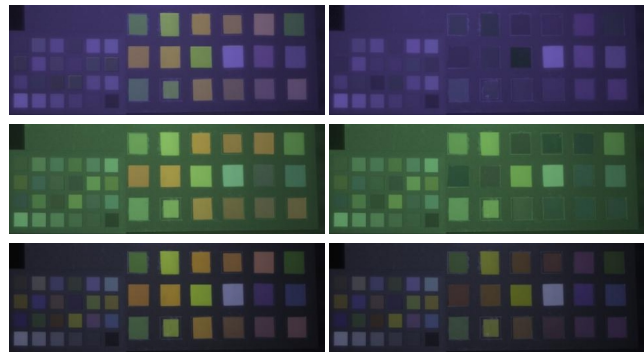
Relighted with Fluorescence   Relighted Reflectance Only

Figure 6: Relighting results for color chart under blue, green, and D250 lights.

Ground Truth   Relighted   Relighted
                 with Fluorescence   Reflectance Only

Figure 7: Relighting results for a scene with fluorescent and non-fluorescent objects under blue, green, and D250 lights.

ities plotted.

Fig. 6 shows relighting results from our color charts. When illuminated with blue light, relighting the scene using only the reflective component results in many fluorescent colors appearing as black. Using our proposed process, the missing colors in the reflectance only image are restored and match the ground truth very accurately. In the D250 illuminated images, the reflectance only case is darker due to the lack of fluorescent emission.

In Fig. 7, we show a scene consisting of a mix of flu-

orescent and non-fluorescent objects. Note that in all the images, the non-fluorescent red and yellow blocks at the top appear the same regardless of whether we consider fluorescence. The fluorescent objects on the other hand, show obvious improvement with our method.

7. Conclusion

We detailed the very different ways reflectance and fluorescence behave concerning emission of light and showed the need for explicit consideration of fluorescence. We also proposed a sparse wavelength imaging method that was successfully applied to the capture of the reflective, emission and excitation components of entire scenes. By applying sparse wavelength imaging to fluorescence, we also showed that fluorescent spectra can be characterized by basis vectors. Finally, we are, to the best of our knowledge, the first to model all aspects of relighting reflective-fluorescent scenes using established theories on the physical behavior of reflectance and fluorescence.

8. Acknowledgment

References

[1] M. Alterman, Y. Schechner, and A. Weiss. Multiplexed fluorescence unmixing. In *ICCP10*, pages 1–8, 2010. 2

[2] K. Barnard. Color constancy with fluorescent surfaces. In *CIC*, pages 257–261. IS&T/SID, 1999. 1, 2

[3] C. Chi, H. Yoo, and M. Ben-Ezra. Multi-spectral imaging by optimized wide band illumination. *IJCV*, 86(2-3):140–151, Jan. 2010. 1, 2

[4] J. M. DiCarlo, F. Xiao, and B. A. Wandell. Illuminating illumination. In *CIC*, pages 27–34. IS&T/SID, 2001. 1

[5] N. Gat. Imaging spectroscopy using tunable filters: A review. In *Wavelet Applications VII*, volume 4056, pages 50–64. SPIE, 2000. 2

[6] M. B. Hullin, J. Hanika, B. Ajdin, H.-P. Seidel, J. Kautz, and H. P. A. Lensch. Acquisition and analysis of bispectral bidirectional reflectance and reradiation distribution functions. *SIGGRAPH 2010*, 29(4):97:1–97:7, 2010. 2, 4

[7] G. M. Johnson and M. D. Fairchild. Full-spectral color calculations in realistic image synthesis. *IEEE Comput. Graph. Appl.*, 19(4):47–53, July 1999. 1

[8] T.-W. Lee, T. Wachtler, and T. J. Sejnowski. The spectral independent components of natural scenes. In *First IEEE Intl. Workshop on Biologically Motivated Computer Vision*, BMVC '00, pages 527–534, London, UK, 2000. Springer-Verlag. 4

[9] L. T. Maloney. Evaluation of linear models of surface spectral reflectance with small numbers of parameters. *JOSA A*, 3(10):1673–1683, Oct 1986. 4

[10] L. T. Maloney and B. A. Wandell. Color constancy: a method for recovering surface spectral reflectance. *JOSA A*, 3(1):29+, 1986. 1, 2

[11] D. H. Marimont and B. A. Wandell. Linear models of surface and illuminant spectra. *JOSA A*, 9(11):1905–1913, Nov 1992. 4

[12] W. Matusik, H. Pfister, M. Brand, and L. McMillan. Efficient isotropic BRDF measurement. In *EGRW*, pages 241–247, Aire-la-Ville, Switzerland, Switzerland, 2003. Eurographics Association. 4

[13] G. McNamara, A. Gupta, J. Reynaert, T. D. Coates, and C. Boswell. Spectral imaging microscopy web sites and data. *Cytometry*, 69A(8):863–871, 2006. 4

[14] J. Park, M. Lee, M. D. Grossberg, and S. K. Nayar. Multispectral Imaging Using Multiplexed Illumination. In *ICCV*. IEEE, Oct 2007. 1, 2

[15] J. P. S. Parkkinen, J. Hallikainen, and T. Jaaskelainen. Characteristic spectra of munsell colors. *JOSA A*, 6:318–322, 1989. 4

[16] M. S. Peercy. Linear color representations for full spectral rendering. In *SIGGRAPH-93*, pages 191–198, Anaheim, CA, 1993. 1

[17] F. W. Rost. *Fluorescence Microscopy*. Cambridge University Press, 1992. 1

[18] I. Sato, T. Okabe, and Y. Sato. Bispectral photometric stereo based on fluorescence. In *CVPR*, pages 270–277. IEEE, 2012. 3

[19] D. A. Skoog, F. J. Holler, and S. R. Crouch. *Principles of Instrumental Analysis*. Thomson Publishers, 2007. 1

[20] A. Springsteen. Introduction to measurement of color of fluorescent materials. *Analytica Chimica Acta*, 380(2–3):183–192, 1999. 2

[21] S. Tominaga. Multichannel vision system for estimating surface and illumination functions. *JOSA A*, 13(11):2163–2173, Nov 1996. 1, 2

[22] S. Tominaga, T. Horiuchi, and T. Kamiyama. Spectral estimation of fluorescent objects using visible lights and an imaging device. In *CIC*. IS&T/SID, 2011. 2

[23] T. Treibitz, Z. Murez, B. G. Mitchell, and D. J. Kriegman. Shape from fluorescence. In *ECCV (7)*, pages 292–306, 2012. 3

[24] G. Ward and E. Eydelberg-Vileshin. Picture perfect RGB rendering using spectral prefiltering and sharp color primaries. In *EGRW*, pages 117–124, Aire-la-Ville, Switzerland, Switzerland, 2002. Eurographics Association. 1

[25] F. Yasuma, T. Mitsunaga, D. Iso, and S. Nayar. Generalized Assorted Pixel Camera: Post-Capture Control of Resolution, Dynamic Range and Spectrum. Technical report, Columbia University, Nov 2008. 6

[26] C. Zhang and I. Sato. Separating reflective and fluorescent components of an image. In *CVPR*, pages 185–192. IEEE, 2011. 2, 3